Performance of the Fermi Large Area Telescope

Riccardo Rando (University & INFN of Padova, Italy)
on behalf of the Fermi Large Area Telescope Collaboration

Summary: We describe the current top-level performance of the LAT. A plan for future developments is also discussed.

Abstract

The current status of the Large Area Telescope (LAT) performance represents the Fermi collaboration's best knowledge of the instrument: calibrations are now based on flight data, and a description of on-orbit effects related to the background event rate is included. We summarize the top-level performance of the LAT as it is currently parametrized and distributed for science analysis. From the performance characterization we derive the LAT point source sensitivity as a function of energy and celestial coordinates. A plan for future developments is also detailed.

LAT event analysis procedures

LAT **response** is defined by the on-board triggering and filtering, on-ground event reconstruction and data analysis procedure.

After triggering and on-board filtering, accepted candidate photons are downlinked to Earth, where they undergo the full **event reconstruction** and **data analysis**. In this stage several different estimates for the direction and energy of the primary are calculated. The best determination of the event direction and energy are chosen using **automated classification algorithms**; for both figures the probability of being in the core of the corresponding distribution is calculated. Then, an additional **background rejection** stage is performed, improving the on-orbit filtering: the probability of the event being a γ is evaluated. All the algorithms used in these stages are **trained on detailed Monte Carlo simulations**.

Event classes are defined in terms of cuts on the high-level parameters we have defined, obtaining a purer dataset (in terms of γ rays) with enhanced spatial and energy resolution as the cuts become harder and harder. The obvious trade-off is between efficiency, purity and resolution.

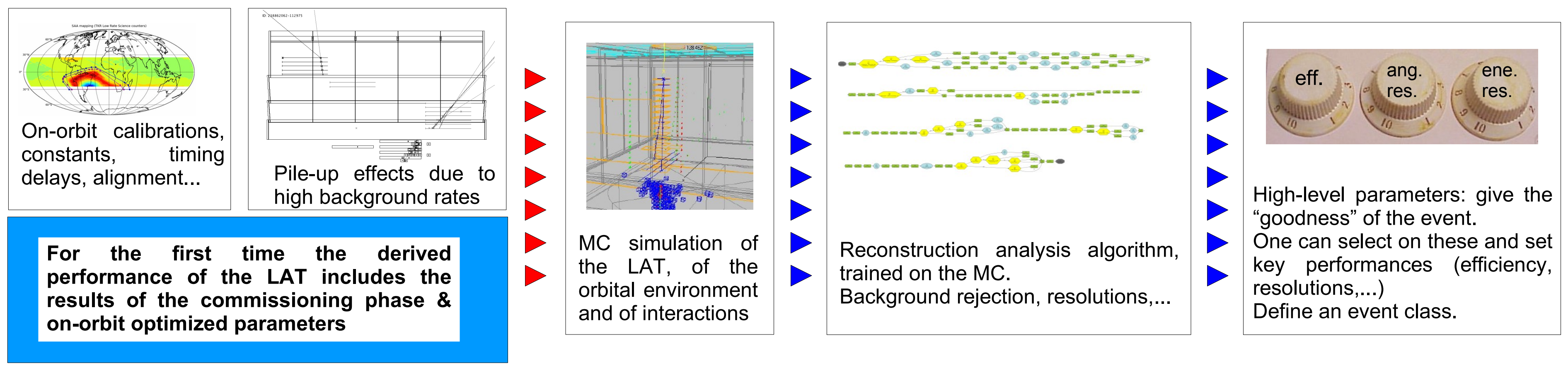

On-orbit calibrations, constants, timing delays, alignment...

Pile-up effects due to high background rates

For the first time the derived performance of the LAT includes the results of the commissioning phase & on-orbit optimized parameters

MC simulation of the LAT, of the orbital environment and of interactions

Reconstruction analysis algorithm, trained on the MC.
Background rejection, resolutions,...

High-level parameters: give the "goodness" of the event.
One can select on these and set key performances (efficiency, resolutions,...)
Define an event class.

On-orbit performance

Detector calibrations affect all aspects of LAT observations, from direction and energy measurement to absolute timing. The on-orbit calibration effort started immediately after Fermi 's launch and the first results are described in great detail in a dedicated paper. Performed calibrations include synchronization of trigger signals, optimization of delays for latching data, determination of detector thresholds, gains and responses, evaluation of the perimeter of the South Atlantic Anomaly (SAA), measurements of live time and of absolute time and internal and spacecraft boresight alignments. **The results of on-orbit calibrations are currently included in the Monte Carlo description of the instrument.**

While examining downlinked events it become clear that some unexpected interactions between background and γ events happened, due to the time evolution of the energy deposition in the detector, the timing of the electronics and of the trigger system, and the details of the reconstruction analysis. This was not observed in Monte Carlo simulation as each event is generated independently and interactions between subsequent events is not possible. This causes a decrease in the LAT efficiency, as some valid events are rejected due to pile-up signals. While we are applying corrections to the reconstruction and event analysis routines to recover this loss, currently **pile-up effects are introduced in our Monte Carlo simulations by superimposing to "pure Monte Carlo" events "real-life data" events** obtained on-orbit with a periodic trigger. These modifications, while not solving the issue, allow us to use the Monte Carlo simulation to correctly estimate the LAT performance and reduce the systematics affecting our science analysis.

LAT response

The LAT response is expressed by means of **instrument response functions** (IRFs). Canonically the detector response is factored into three terms: efficiency in terms of the detector **effective area**, and resolutions as **point spread function** and **energy dispersion**. Components of the IRFs are usually a tabular representation of the corresponding figures of merit in terms of the photon true energy and direction in the detector system of reference.

To evaluate the LAT response a **dedicated Monte Carlo simulation** is performed. A huge amount of γ events is simulated, in order to cover with good statistics all possible photon inclinations and energies.

Pre-launch performance estimates and related IRF set were called "**P6_V1**", here we document "**P6_V3**", the first response functions including **post-launch calibrations** and additional **orbital effects**.

Instrument response for class P6_V3_DIFFUSE

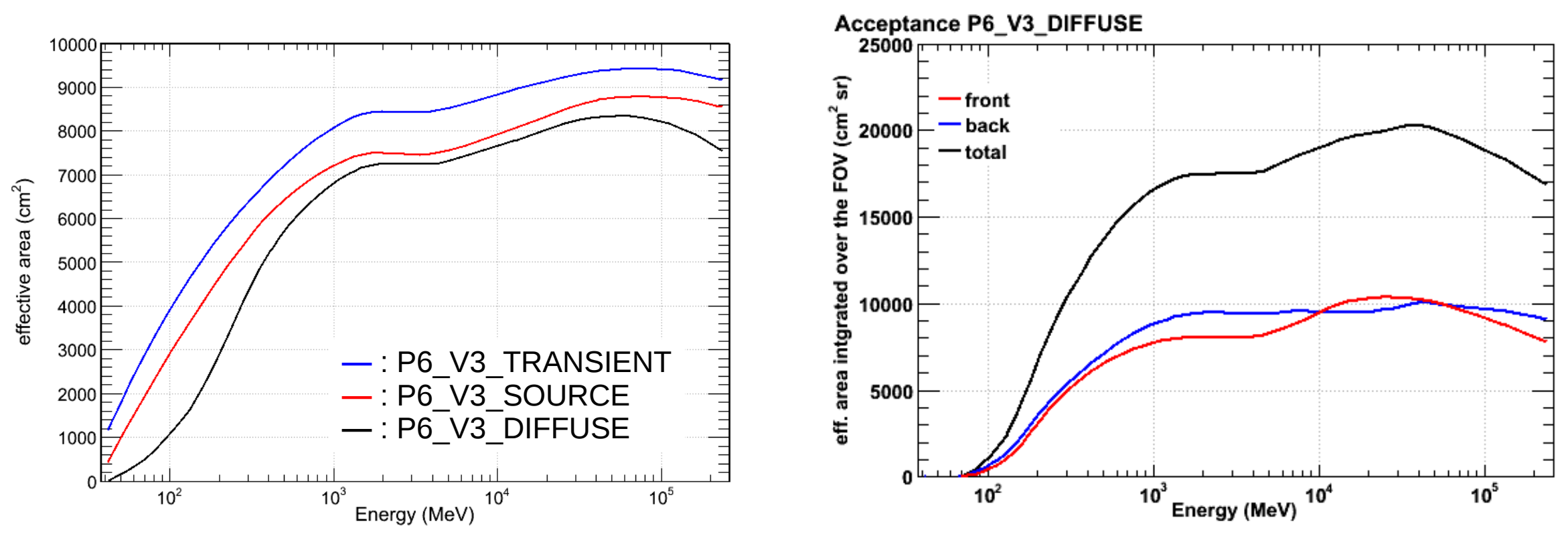

Left: effective area for normally incident photons. The three standard event classes are shown: to a smaller efficiency corresponds a smaller residual background rate: about 2 Hz for "transient", 0.5 Hz for "source" and 0.1 Hz for "diffuse".
The effective area is smaller at low energy with respect to previously quoted performances due to event pile-up; the difference is within quoted systematics.

Right: acceptance, i.e. effective area integrated across the Field-Of-View, for the P6_V3_DIFFUSE class.

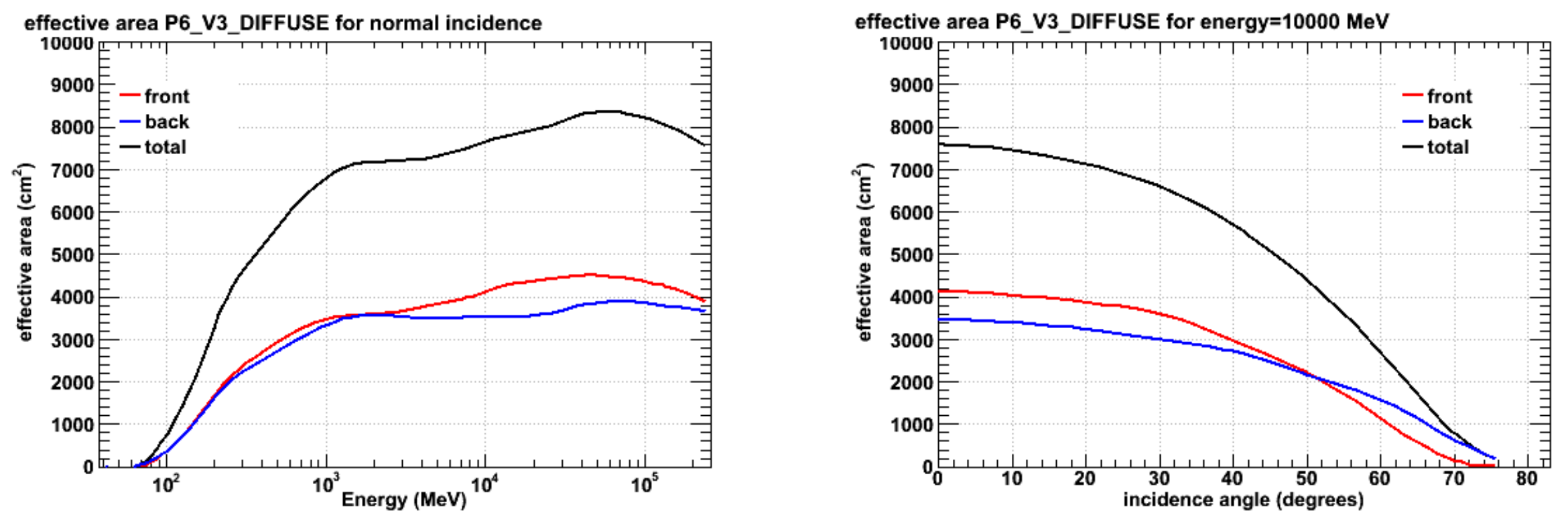

Effective area (aeff) for class P6_V3_DIFFUSE.
Left: effective area vs. photon true energy for normal incidence. Front and back indicate whether the photon interacted in one of the thin conversion layers (3% r.l.) or in the thick layers (18% r.l.). Currently systematics on P6_V3_DIFFUSE effective area are estimated to be 10% at 100 MeV, 5% at 500 GeV and 20% at 10 GeV.
Right: effective area vs. incidence angle for 10 GeV photons.

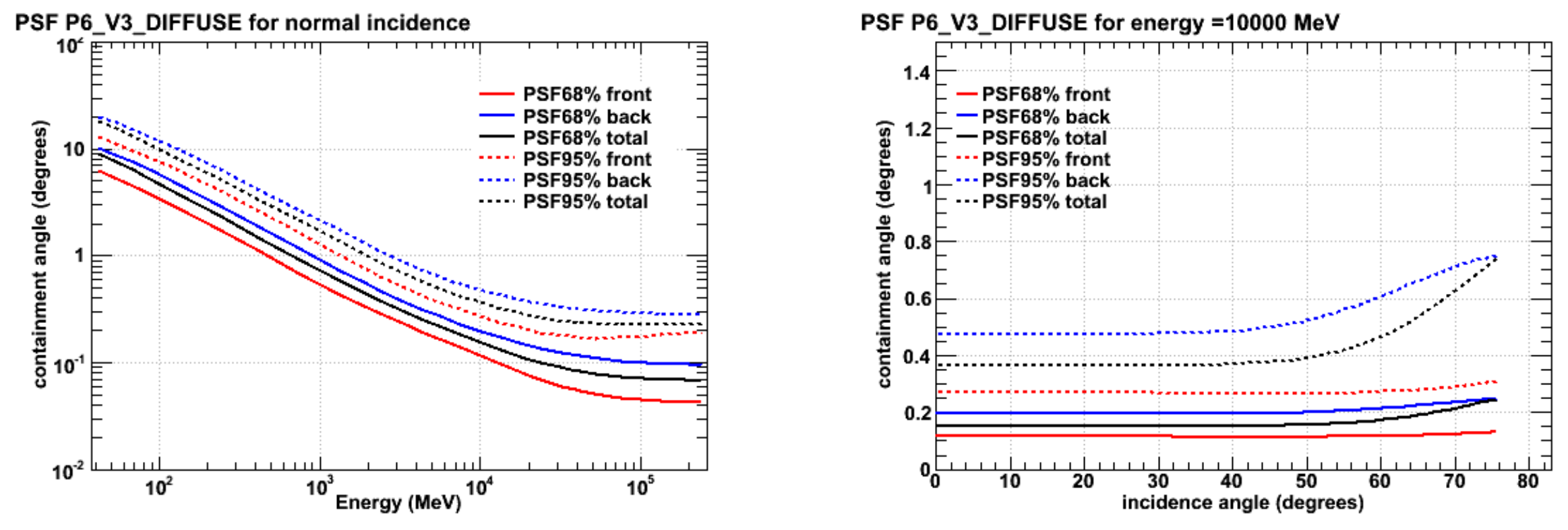

Point spread function (PSF) for class P6_V3_DIFFUSE.
Left: PSF vs. energy for normal incidence photons: 68% and 95% containment are shown for front- and back-converting photons, and the aeff-weighted average is also shown. The power-law decrease indicates the dependence on multiple scattering at lower energy, while at higher energy the PSF saturates at a value given by the tracker segmentation. The effect of event pile-up on the angular resolution is negligible.
Right: PSF vs. incidence angle for 10 GeV photons.

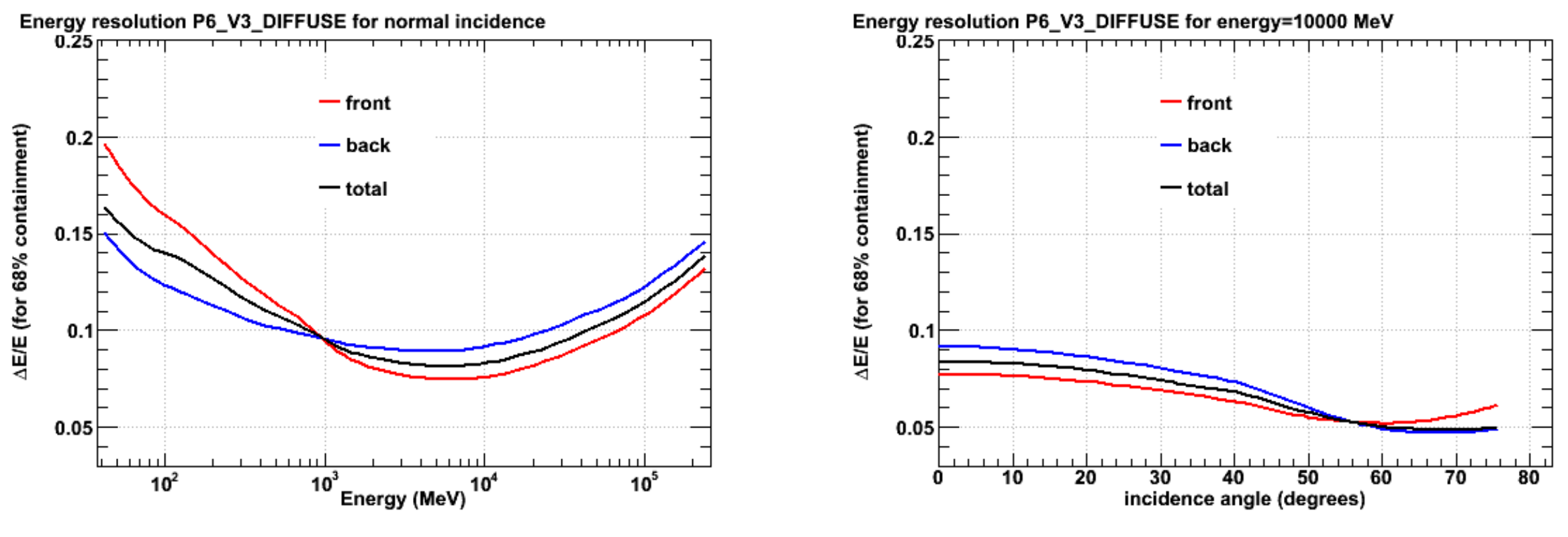

Energy dispersion (edisp) for class P6_V3_DIFFUSE.
Left: 68% containment level vs. energy for normal incident photons is shown for front- and back-converting photons, and the aeff-weighted average is also drawn.
Right: edisp vs. incidence angle for 10 GeV photons.

High-level performance for class P6_V3_DIFFUSE

This first plot shows the differential sensitivity for an isolated, high-latitude point source. The differential sensitivity is evaluated from the 5σ sensitivity limit for 1/4-decade ranges of energy. Quantitatively, the 5σ limit is taken as the likelihood test statistic of 25.
Limits are derived in each energy range **independently** and are based on a live time of 0.8 yr, which is the approximate value for a 1-year data set; this takes into account the loss of observing time due to: SAA passages and the instrumental deadtime, that the observations are in survey mode; and that the diffuse background is isotropic and has an intensity of 1.5 x 10^{-5} cm^{-2} s^{-1} sr^{-1} (>100 MeV) and a photon index of 2.1. Also shown are curves for background intensities that are 10x and 100x greater; the latter roughly approximating the intensity near the Galactic center.

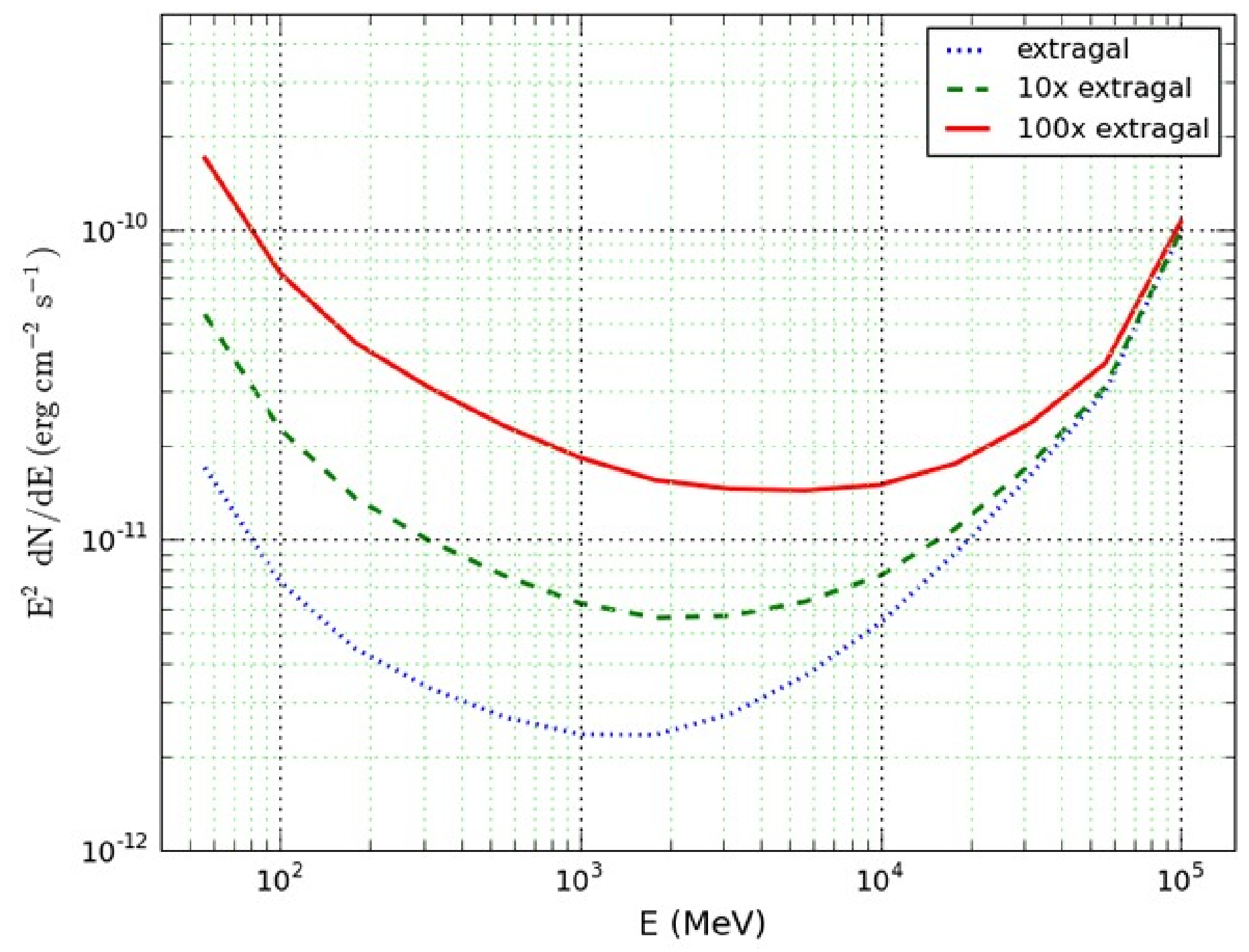

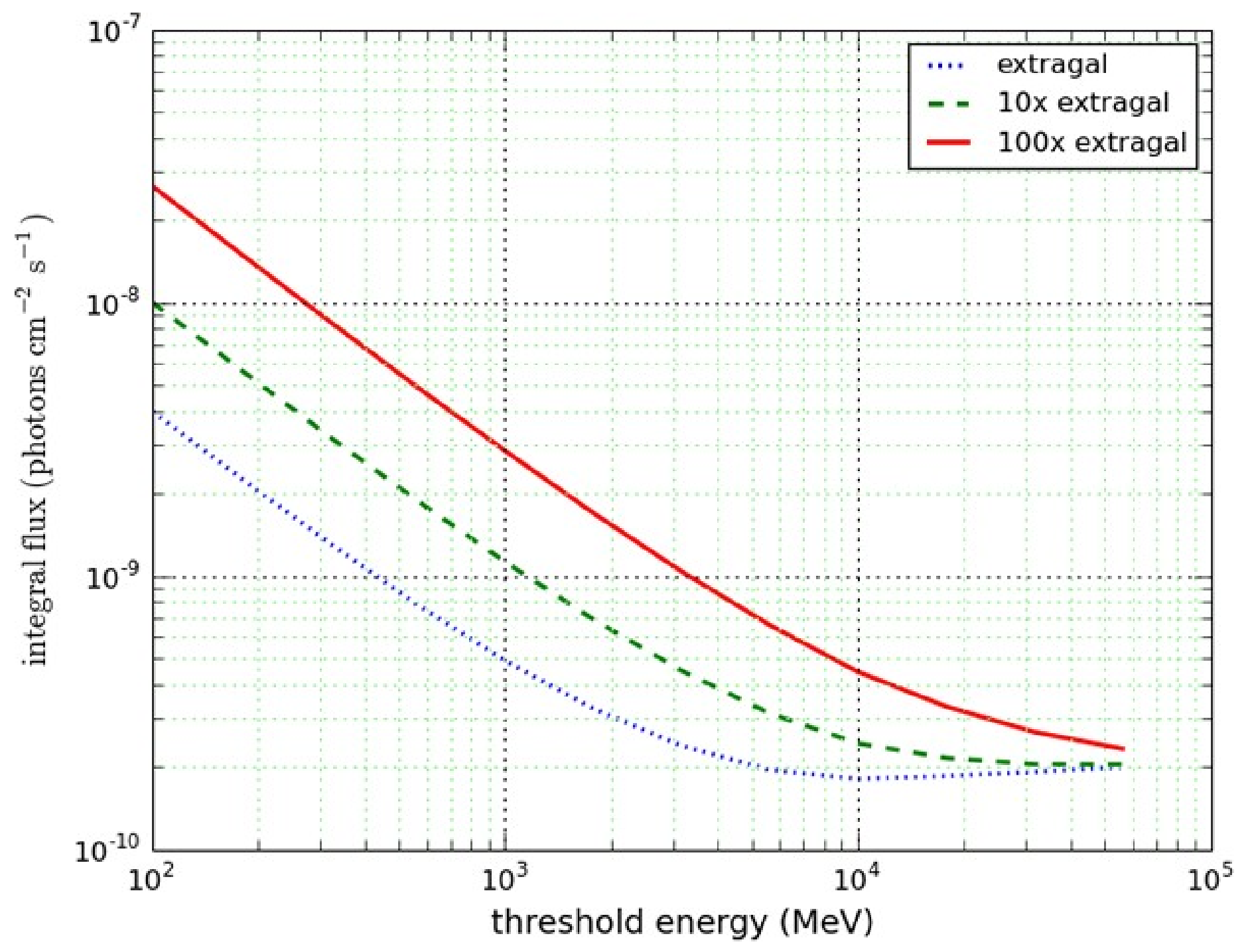

Experiments are often compared using an integral sensitivity plot (5σ sensitivity for $E>E_0$), assuming a $1/E^2$ spectrum source at high latitude. Other parameters are the same used for the previous plot.

There are also significant variations of the sensitivity due to the spatial structure in the diffuse galactic gamma-ray background. These are summarized in the map on the right, which shows the 5σ sensitivity across the sky in Galactic coordinates. We calculated the significance for a point source with spectral index -2.0, a standard galactic diffuse model and an ad-hoc description of the isotropic emission (true EGB emission + residual background) for a 1-year observation in survey mode.

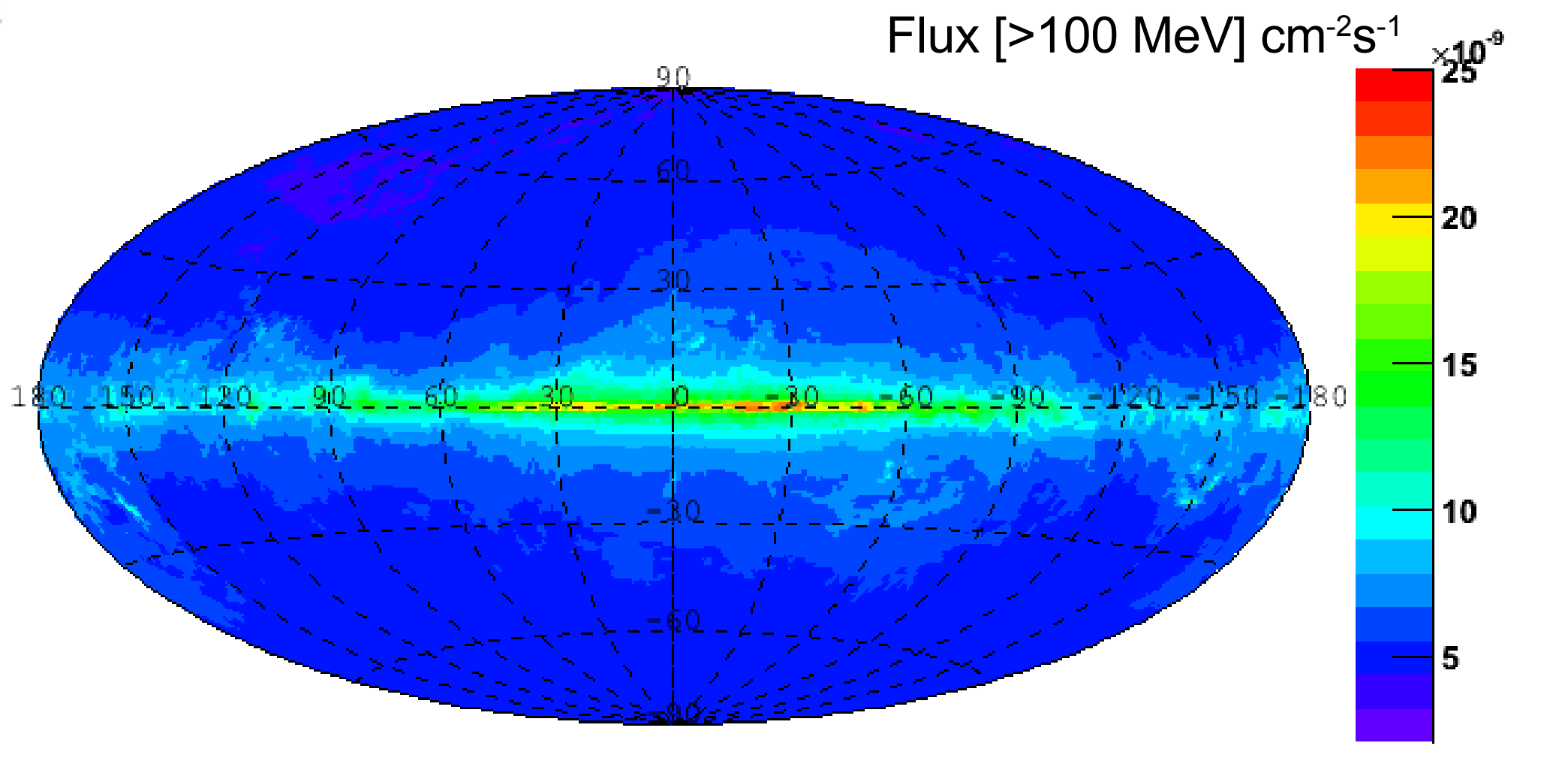

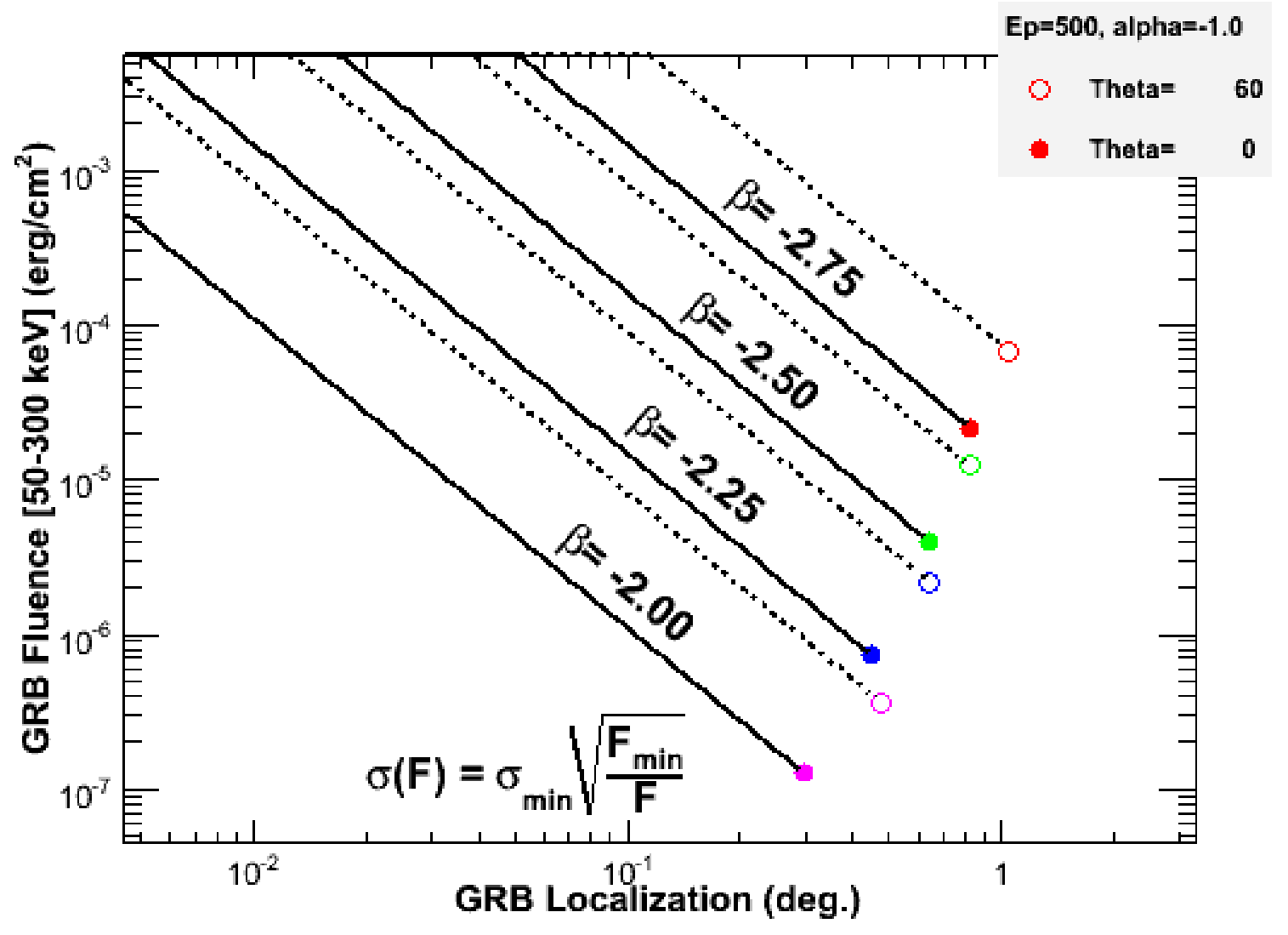

An estimator for the GRB localization power as a function of the fluence. GRB is assumed to have a Band-law spectrum with spectral index α=-1.0 before the peak at E_{peak}=500 keV.
Each marker corresponds to a different inclination angle and a different high energy spectral index, and represents the minimum fluence (in the standard 50 keV - 300 keV energy band), which corresponds to a detection (y-axis) vs the 68% localization accuracy (x-axis). The solid and dotted lines are the result of the formula shown on the canvas, and allow computation of the localization at a given fluence (for normal incidence and for 60 degrees off-axis).

Future developments

Event analysis routines are currently being updated to into a new scheme ("**P7**"). This will include a dedicated analysis of background events like electrons, protons and heavy ions; several new event classes will be made available for science analysis. Moreover, all automated predictors and classifiers used in the analysis scheme will be retrained using Monte Carlo datasets including pileup effects. In addition, steps are being taken to manage the presence of ghost-affected events within the reconstruction and event analysis stages as it was successfully demonstrated that ghost tracks in the tracker can be recognized and tagged, while a new clustering scheme in the calorimeter is being investigated; these developments are post-P7 though: to find more about this see **L. Rochester's and Tracy Usher's posters** at this symposium.

We have now enough statistics to derive the instrument angular resolution from celestial high-latitude point sources. The current development plan implies that future IRFs sets will include a real-data derived PSF parametrization. To find out more about this see **T. Burnett's poster** at this symposium.

Conclusions

After the early calibration phase the first on-orbit performance estimates for *Fermi* LAT are evaluated. Currently the LAT response suffers from some degradation due to residual energy depositions caused by the high background particle rate, rather evident in the case of the effective area, and it is to be considered not yet optimal. This is currently described by the release of the IRF set described in this contribution. We have documented the current status of reconstruction and data analysis, and we discussed the future updates being implemented to recover more of the full capability of the LAT.

References:

http://www-glast.slac.stanford.edu/software/IS/glast_lat_performance.htm
W.B. Atwood et al., *The Large Area Telescope on the Fermi Gamma-ray Space Telescope Mission*, ApJ 697, 6/2009
L. Baldini et al., *Preliminary results of the LAT Calibration Unit beam tests*, The First Glast Symposium. AIP Conf. Proc., Vol. 921, 2007
A. Abdo et al., *On-orbit calibration of the Fermi Large Area Telescope*, submitted to Astroparticle Physics, arXiv:0904.2226
R. Rando, *Post-launch performance of the Fermi Large Area Telescope*, arXiv:0907.0626

Acknowledgments:

The *Fermi* LAT Collaboration acknowledges support from a number of agencies and institutes for both development and the operation of the LAT as well as scientific data analysis. These include NASA and DOE in the United States, CEA/Irfu and IN2P3/CNRS in France, ASI and INFN in Italy, MEXT, KEK, and JAXA in Japan, and the K. A. Wallenberg Foundation, the Swedish Research Council and the National Space Board in Sweden. Additional support from INAF in Italy for science analysis during the operations phase is also gratefully acknowledged.

2009 Fermi Symposium - 2–5 November 2009 - Washington DC